Title
Mineral Scaling in 3D Interfacial Solar Evaporators—A Challenge for Brine Treatment and Lithium Recovery.

Journal
Environmental Science & Technology, 59(1)

Authors
Eskafi, Aydin
De Finnda, Casey
Garcia, Christopher
et al.

Publication Date
2025-01-14

DOI
10.1021/acs.est.4c08151

Peer reviewed

Environmental Science & Technology

pubs.acs.org/est

Article

Mineral Scaling in 3D Interfacial Solar Evaporators—A Challenge for Brine Treatment and Lithium Recovery

Aydin F. Eskafi, Casey De Finnda, Christopher A. Garcia, and Baoxia Mi*

Cite This: *Environ. Sci. Technol.* 2025, 59, 892−901

Read Online

ACCESS | Metrics & More | Article Recommendations | Supporting Information

ABSTRACT: In this work, we analyzed the effects of mineral scaling on the performance of a 3D interfacial solar evaporator, with a focus on the cations relevant to lithium recovery from brackish water. The field has been rapidly moving toward resource recovery applications from brines with higher cation concentrations. However, the potential complications caused by common minerals in these brines other than NaCl have been largely overlooked. Therefore, in this study, we thoroughly examined the effects of two common cations (calcium and magnesium) on the long-term solar evaporation performance of a 3D graphene oxide stalk. The 3D stalk can achieve an evaporation flux as high as 17.8 kg m^{-2} h^{-1} under one-sun illumination, and accumulation of NaCl on the stalk surface has no impact. However, the presence of $CaCl_2$ and $MgCl_2$ significantly reduces the evaporative flux even in solutions lacking scale-forming anions. A close examination of scale formation during long-term evaporation experiments revealed that $CaCl_2$ and $MgCl_2$ tend to precipitate out within the stalk, thus blocking water transport through the stalk and significantly dropping the evaporation rates. These findings imply that research attention is needed to modify and optimize the internal water transport channels for 3D evaporators. Additionally, we emphasize the importance of testing realistic mixtures—including prominent divalent cations— and testing long-term operations in interfacial solar evaporation research and investigating approaches to mitigate the negative impacts of divalent cations.

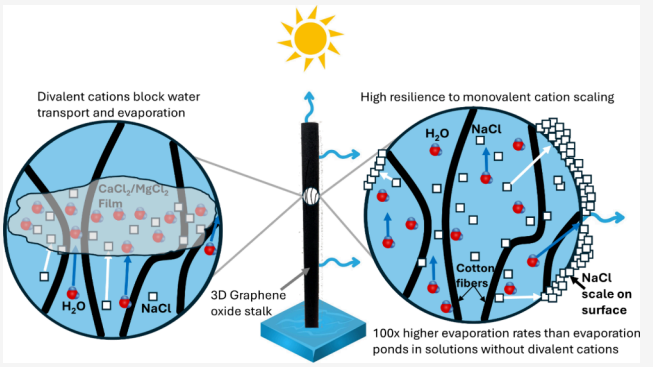

KEYWORDS: *Interfacial solar evaporation, 3D evaporator, solar desalination, graphene oxide, divalent cation scaling, lithium recovery, solar resource recovery*

INTRODUCTION

Interfacial solar evaporation is an emerging method for passively increasing the evaporation rate of water allowing for sustainable desalination and resource recovery applications. As global water scarcity increases, the technology can allow for passive desalination with zero-liquid discharge as well as sustainable capture of valuable salts that exist in brines. Recent research in this field has focused on 3D evaporators, which have a higher evaporative surface, leading to evaporative fluxes over ten times greater than comparable 2D materials.[1,2] These evaporators continuously wick water onto elevated surfaces through capillary forces. The water can then evaporate from the surfaces of the material as it absorbs photothermal energy from the sun. Many different materials have been proposed for evaporators including various types of plasmonic, semiconducting and carbon based materials.[3] Carbon based materials such as graphene oxide (GO),[1,4,5] carbon nanotubes,[6−8] and biochar-based compounds[9−12] have been particularly widely used due to their inexpensive precursors, intrinsically high solar absorption capacities, and resulting high evaporative fluxes. Among the different designs of solar evaporators, 3D designs such as cylinders,[1,13] cones,[2,6,14] and cups[15] stand out due their advantages in drastically increasing the evaporation surface area and thus the evaporative flux. Our previous research has shown that a 3D graphene oxide (3D GO) stalk consisting of a cylindrical cotton stick coated with GO through a cross-linking process leads to a consistently high evaporation rate and resists negative effects associated with sodium chloride scaling at concentrations as high as 17.5 wt % NaCl.[1]

Initial applications of interfacial solar evaporation focused on passive solar desalination. However, recently resource recovery applications have become more prominent due to the high value of many of the salts found in brines.[16,17] Many naturally occurring and desalination brines include high concentrations of valuable ions such as lithium, boron, and magnesium. Interfacial solar evaporation materials can be modified to

Received: August 6, 2024
Revised: December 18, 2024
Accepted: December 19, 2024
Published: January 2, 2025

capture these valuable ions during evaporation of the brine water. Lithium is a particularly attractive candidate for capture due to the large projected growth in demand for lithium ion batteries over the next 20 years and since the majority of the world's lithium supply exists in salt-lake brines.[18,19] Two recent studies showed high lithium recoveries from brines using interfacial solar evaporation.[20,21] However, the effects of mineral scaling in those systems has not been sufficiently addressed.

Different salts may exhibit different crystallization behavior and affect the performance of the interfacial solar evaporation process, because the solution becomes supersaturated on the evaporator surface as water evaporates and nucleation becomes thermodynamically favored.[22−24] Studies done evaporating droplets have characterized the mechanisms of salt crystallization and shown that evaporation characteristics vary depending on the type of salts.[25,26] For example, one study evaluated the evaporation of droplets of calcium chloride and showed that it displays an "oscillating" behavior where its films absorb and desorb water.[27] Another study investigated sodium chloride droplets, and found that the salt crystals exhibit a unique behavior where they self-eject from their substrate material as the droplets evaporate.[28]

To date, most solar evaporation studies on scaling have focused on sodium chloride alone. Typically, the evaporation rate of a solution is expected to decrease as the salt concentration increases due to a decrease in the vapor pressure of the solution. However, many solar evaporation materials show no corresponding decline as the NaCl concentration increases.[1,8,23,29] Different materials and systems, including Janus membranes,[30−32] localized crystallization systems,[6,33] and self-cleaning materials,[34−36] have been investigated in regards to NaCl scaling. These systems have been extensively summarized elsewhere.[23,29,37,38] Despite these innovations, the effects of nonsodium cations on solar evaporation performance have not been adequately investigated and this remains a major issue that must be addressed prior to commercialization of the technology.

Many of the salt-lake brines that have high potential for resource recovery using solar evaporation have high concentrations of divalent cations. For example, in lithium containing brines the concentration of magnesium can be as high as 3 wt % and the concentration of calcium can be as high as 2.4 wt %.[39,40] Table S1 summarizes the ion concentrations of selected lithium containing brines throughout the world. In commercialized processes, such as the chemical precipitation method currently used for lithium mining, reducing the concentration of the divalent cations is the costliest step as they can prevent high lithium recoveries from some brines.[18,41,42] Studies in membrane systems have also shown that calcium and magnesium are significant causes of flux declines due to inorganic scaling.[24,43] One previous study investigated the solar evaporation performance of a box-like structure in concentrated seawater solutions. They found that at high concentrations, magnesium sulfate scaling can cause a decrease in the evaporation rate.[44] Those findings further indicate the importance of studying nonsodium cations. However, most brine solutions contain much higher concentrations of chloride salts than sulfate salts and some contain high calcium concentrations without correspondingly high amounts of magnesium. The impacts of calcium and the chloride analogs of divalent cations on the solar evaporation process have not been previously investigated. This, along with the previously mentioned differing crystallization effects suggests that these divalent cations can significantly affect the performance of interfacial solar evaporation systems. However, this effect has not been adequately studied or characterized.

In this work, the scaling effects of divalent cations on the evaporation performance of a 3D GO stalk were systematically evaluated. The 3D GO stalk was synthesized using a simple, cost-effective method and it exhibited high evaporative flux rates even in solutions with high NaCl concentrations. In order to evaluate potential resource recovery applications, we conducted a series of long-term experiments with brine solutions containing high concentrations of magnesium and calcium. During these long-term experiments, we closely monitored the evaporative flux as well as the scale formation on the stalk. The distribution, morphology and composition of the scale were characterized using scanning electron microscopy (SEM), energy dispersive X-ray spectroscopy (EDS), and X-ray diffraction (XRD). The results from this paper show that the scaling behavior of sodium chloride alone is not representative of brines in interfacial solar evaporation due to the effects of divalent cations. They illustrate that even the highly soluble chloride salts of divalent cations lead to large drops in evaporative flux. These findings are especially relevant as the field of interfacial solar evaporation moves toward resource recovery from concentrated brine solutions.

METHODS

Material Synthesis. A cylindrical cotton stalk, (0.75 cm diameter, 20.9 cm height) was coated with polydopamine (PDA) and then GO over 4 days. Initially, a solution was prepared by combining 0.25 mL of 1 M Tris(hydroxymethyl) aminomethane hydrochloride (Tris-HCl) and 50 mg of dopamine hydrochloride into a beaker containing 24.75 mL of deionized (DI) water. The resulting solution was mixed until dissolved, and a pink hue developed. The cotton stalk was then submerged in the PDA solution and shaken at 150 rpm for 24 h, ensuring uniform coating of the stalk. The PDA coated stalk was then allowed to air-dry. Afterward, a second solution with 1.25 mL of 20 mg/mL GO was added to DI water and the stalks were submerged and then shaken at the same conditions for 24 h. After developing an even PDA-GO coating, the PDA-GO coated stalk (3D GO stalk) was heated at 150 °C for an additional 24 h before being washed twice in DI water and air-dried.

Material Characterization. For the sample cross-section images, the stalks were first freeze-dried overnight to remove the water, while retaining the existing salt structures. They were then cut into thin pieces and imaged either in a Phenom Pro Tabletop SEM at 10 kV for the SEM images or in a Zeiss Gemini Ultra-55 fitted with a Bruker X-ray Energy Dispersive Spectrometer at 30 kV for SEM/EDS images. XRD measurements were taken using a Bruker D8-Discover at 30 kV and 40 mA with Co radiation. Thermal images were taken using a Fluke Thermal Imager and analyzed using the Fluke SmartView software.

Brine Preparation. Different brine solutions containing varying concentrations of sodium, calcium, lithium, magnesium, and potassium, were made using their respective salt chloride compounds. The realistic brine solution was a replication of the composition of the Salar de Atacama salt pan in Chile and contained 0.15% Li^+, 7.17% Na^+, 1.85% K^+, 0.96% Mg^{2+}, and 1.46% Ca^{2+}.[45] To study cation effects, we also prepared synthesized brine solutions consisting of 100 g/L of

https://doi.org/10.1021/acs.est.4c08151
Environ. Sci. Technol. 2025, 59, 892−901

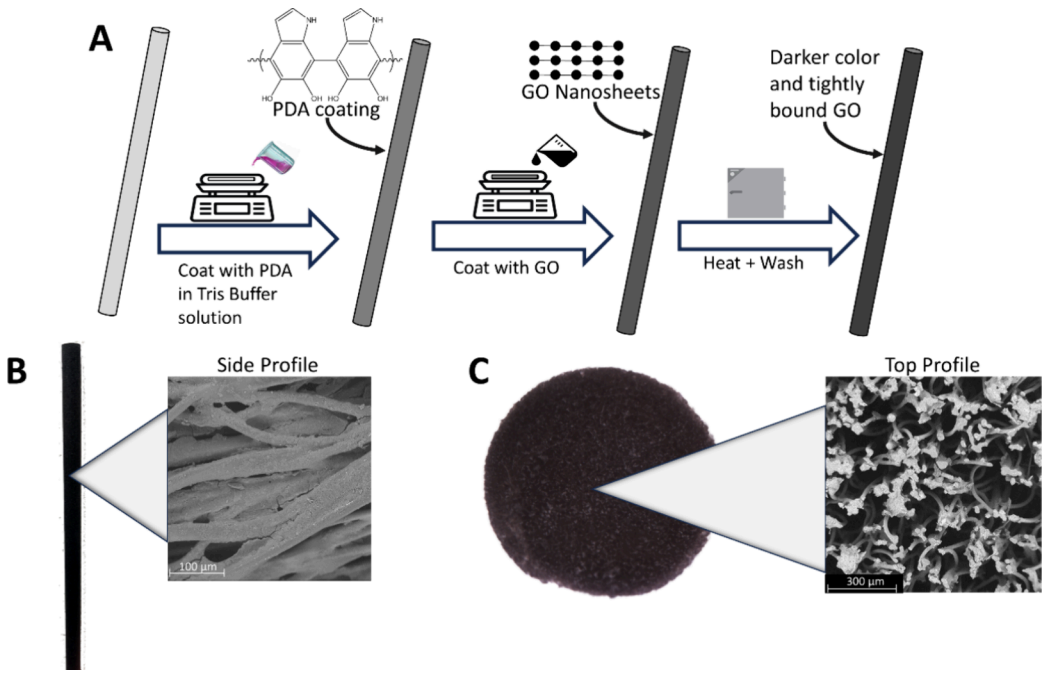

Figure 1. Material synthesis and characterization of the 3D GO stalk including (A) a diagram of the synthesis process for the stalk, (B) optical and SEM image of the side of the GO stalk, and (C) optical and SEM images of a cross-section of the GO stalk.

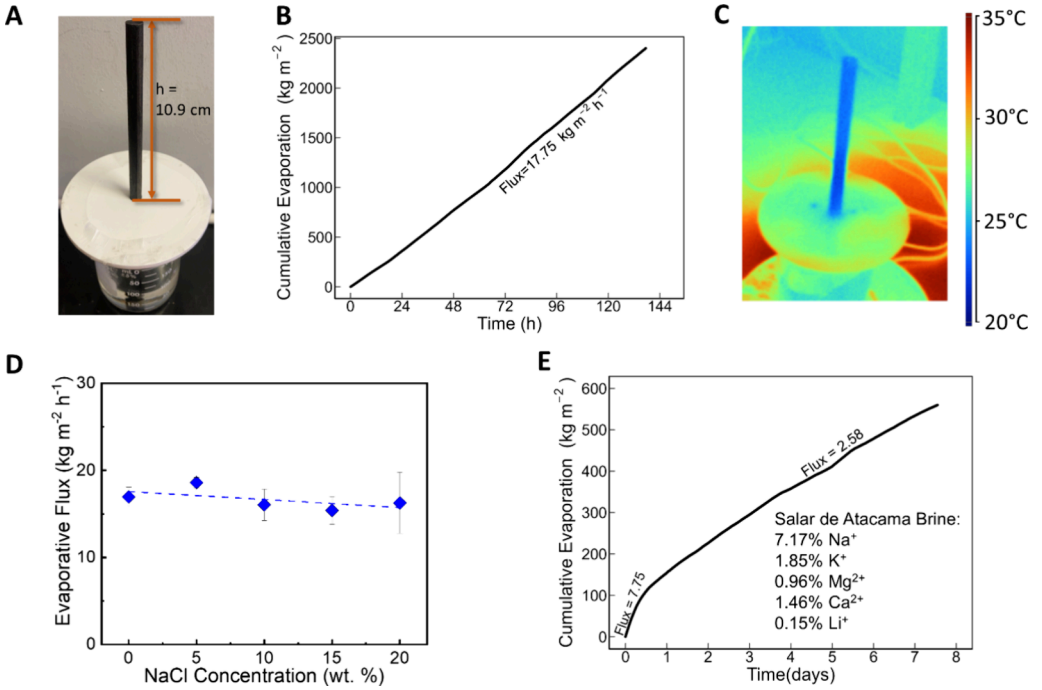

Figure 2. Characterization of the stalk including (A) a visualization of the evaporation setup showing the height of the stalk above the solution, (B) the water evaporation performance of the 3D GO stalk with pure water, (C) a thermal image of the stalk during evaporation, (D) the water evaporation flux of the stalk as the sodium chloride concentration increases, and (E) the water evaporation rate of the stalk (in kg m^{-2} h^{-1}) in a synthetic solution simulating a real brine, the Salar de Atacama Brine in Chile. The anions in all the solutions used in the experiments are chloride ions.

Na^+ and 17 g/L of one of the Ca^{2+}, Mg^{2+}, and K^+. Brine solutions containing only one of the four minerals (Na^+, K^+, Ca^{2+}, and Mg^{2+}) were also investigated at high concentration (100 g/L) to elucidate their unique effects on evaporation under exaggerated conditions.

Solar Evaporation Experiments and Performance. Evaporation experiments were started by placing the 3D GO stalk into a 250 mL beaker filled with 200 mL of the desired brine solution. The stalk was placed through a circular disk with a hole cutout in the center to hold the stalk. The bottom of the stalk stayed submerged in the brine solution to offer a consistent supply of water through the stalk, and the circular disk had its edges wrapped in parafilm to secure the disk and prevent water vapor from escaping.

https://doi.org/10.1021/acs.est.4c08151
Environ. Sci. Technol. 2025, 59, 892−901

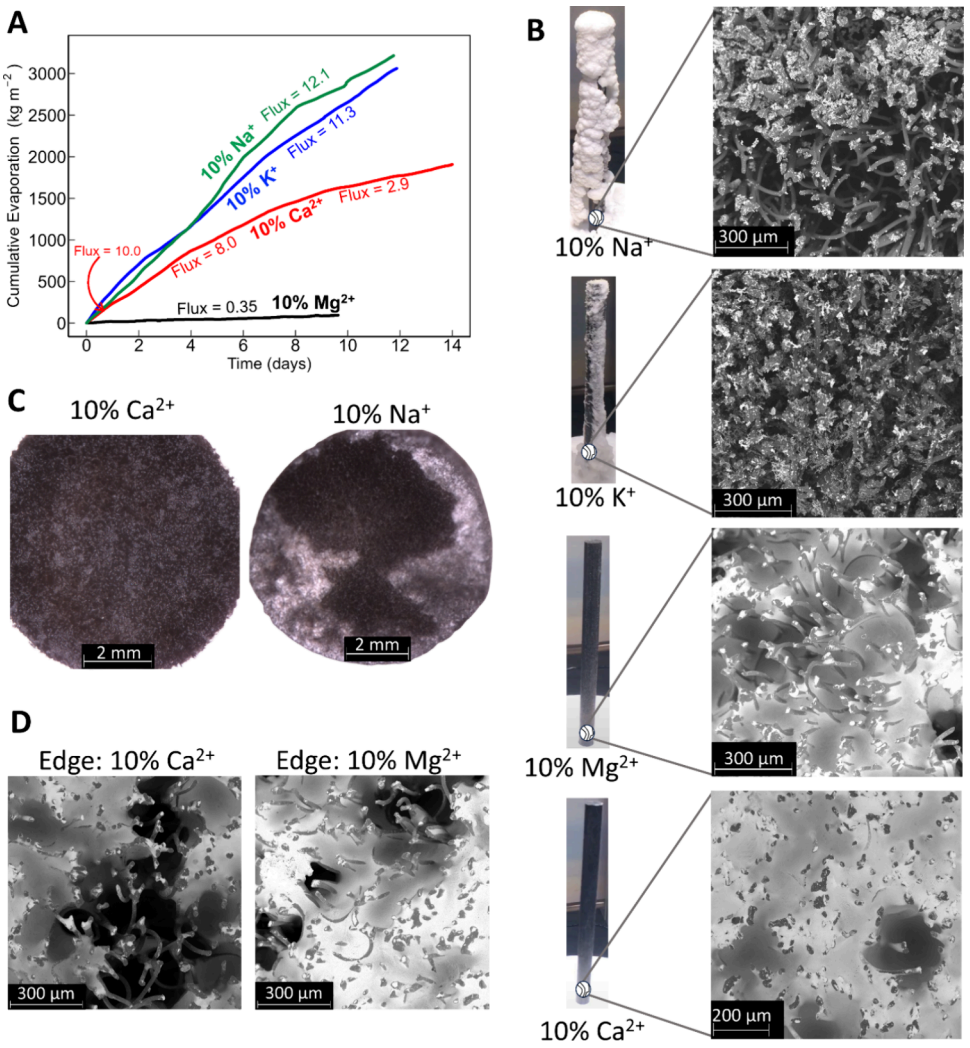

Figure 3. (A) Water evaporation performance of the stalk for solutions containing 10% Na^+, Ca^{2+}, K^+, and Mg^{2+} (flux values are in kg m^{-2} h^{-1}). (B) Images of the scale formation on the outside surface of the stalk for different salt solutions and the cross-section SEM images of the center of each corresponding stalk at a location near the bottom of the stalk (i.e., 9 cm from the top of the stock). (C) Optical cross-section images at the same location of the stalk for solutions containing 10% Ca^{2+} or 10% Na^+. (D) Cross-section SEM images near the edge of the stalk for solutions containing 10% Ca^{2+} or 10% Mg^{2+}. The counterions in all of the experiments are Cl^-.

The solar evaporation performance was evaluated using a solar simulator (G2V Systems) with illumination set at an intensity of 1,000 W/m^2 (1 sun illumination) for all experiments. The mass evaporated was measured every minute using a mass balance and the temperature and humidity were monitored using sensors. The temperature varied from 25 to 35 °C, and the humidity varied from 25 to 40% over the course of the experiments. These variations do not cause notable differences in the evaporative performance of the material. The evaporation rate was then calculated using the top area of the stalk (0.442 cm^2), the height (10.9 cm), and the evaporative area index (59) as previously described.[1]

RESULTS AND DISCUSSION

Synthesis and Characterization of the 3D GO Stalk. To synthesize the 3D GO stalk, we started with commercially available cotton humidifying sticks which were chosen as the substrate material due to their high hydrophilicity, porosity, and low cost. Hydrophilicity and porosity are essential properties for an interfacial solar evaporation material because of the necessity of a constant supply of water in the stalk. The cotton sticks were then coated in a simple three step process as shown in Figure 1A. This process, which only requires the use of a shaker and an oven, is highly scalable. The number of stalks that can be coated at once is solely limited by the size of the container holding the stalks. Polydopamine (PDA), a natural polymer, was chosen as the intermediate polymer due to its low cost, dark color and its ability to tightly bind to both the cotton substrate and the GO. The final product, the 3D GO stalk has a dark exterior which allows for efficient solar and thermal absorption. The images in Figure 1B show a uniform GO coating on the stalk exterior which still retains the pores necessary to allow the water to escape from the interior of the stalk and evaporate. The images of a cross-section of the middle of the stalk in Figure 1C show that the GO fully coats the interior of the stalk as well, while leaving the pores fully open to allow for a high rate of water transport through the stalk. The openings of ~100 μm found in the stalk allow for the rapid lifting of the water which maintains the stalk at saturation over continued operations, allowing for continuously high evaporation rates.

https://doi.org/10.1021/acs.est.4c08151
Environ. Sci. Technol. 2025, 59, 892−901

After synthesizing the 3D GO stalk, we conducted a series of baseline characterization experiments to confirm the high interfacial solar evaporation performance. Figure 2A shows the setup for evaporation experiments. The height of the stalk above water was a relatively high, 10.9 cm. This height was selected to maximize the evaporation area on the sides of the stalk while still allowing for water transport by spontaneous capillary wicking. Figure 2B shows that the pure water evaporation rate of the stalk is 17.75 kg m^{-2} h^{-1}, which represents a flux over 100 times greater than the evaporation rate from the surface of a water body. This is at the high-end of solar evaporator devices found in the literature.[1,46,47] The evaporation rate remains constant over a period of 6 days showing that the stalk can consistently replenish the water supply near the top. This finding is borne out by the thermal images in Figure 2C, which show that the stalk is much colder than the ambient environment due to the high rate of evaporation and water saturation along its entire surface. To test the materials' resilience to sodium chloride scaling, we also conducted 48-h long evaporation experiments with increasing concentrations of sodium chloride. As shown in Figure 2D, when the concentration rises from 0 to 20 wt % (above the concentration found in real brines), the evaporative flux stays relatively constant at around 15 kg m^{-2} h^{-1}. This finding reflects our previous research and shows that sodium chloride scaling will not hinder the use of the stalk in any brine solution.

However, it is important to note that sodium chloride is not typically found alone in salt-lake brines. For example, in lithium recovery applications the brine often contains relatively high concentrations of divalent cations that could potentially affect the evaporation rate. To that end, a synthetic brine solution was made simulating the composition of the Salar de Atacama in Chile which contains one of the largest lithium deposits in the world. As listed in Figure 2E, this solution contained a mixture of calcium, magnesium, sodium and potassium cations as well as lithium. When tested with the 3D stalk, the evaporation rate for the synthetic bine started at around 7.75 kg m^{-2} h^{-1}, which is about half of the rate for a pure NaCl solution at equivalent concentrations. After about 24 h, the evaporation rate further dropped to 2.58 kg m^{-2} h^{-1} and remained relatively stable for the next 7 days. Since we only used chloride ions in our experiments, the drastically slower evaporation for the synthetic solution can only be attributed to the different cations.

Understanding the Effects of Different Cations on the Evaporation Performance and Scale Formation. To single out the effects of different cations on the solar evaporation performance of the stalk, we performed evaporation tests with solutions containing very high concentrations (10 wt %) of the individual cations, Na^+, K^+, Mg^{2+}, and Ca^{2+}. The counterions in all the solutions are Cl^-. We did not continue testing lithium because, as seen in Table S1, it exists at sufficiently low concentrations in the brines that it is not a significant factor affecting the scaling behavior of the solutions. Each experiment lasted over 10 days to observe long-term scaling effects. Note that a 10% concentration is higher than what would be expected in most natural brines, but this high concentration was chosen to accelerate the scaling effects to elucidate the mechanisms involved.

The results in Figure 3A show that calcium and magnesium ions significantly decrease the evaporation rates. The stalk has high resistance to potassium and sodium scaling with the evaporative flux staying above 11−12 kg m^{-2} h^{-1} over 12 days of continuous evaporation under the solar simulator. Meanwhile, the evaporative flux for calcium solution started at a similar value as that of sodium or potassium, but it continuously declined by nearly 3-fold over the course of the experiment (around 14 days). The effect of magnesium ions is interestingly more severe than that of calcium. As shown in Figure 3A, the evaporative flux for magnesium was at a very low value of 0.35 kg m^{-2} h^{-1} even from the beginning of the experiment, and this flux is only about 3% of that of sodium or potassium.

Interestingly, the high-flux salts (NaCl and KCl) exhibited significant scale accumulation on the outside surface of the stalk during evaporation, while the low-flux salts ($CaCl_2$ and $MgCl_2$) showed very little accumulation. As shown by the stalk images in Figure 3B, taken after 10 days of evaporation, as well as the videos in Supplementary Movie S1, sodium and potassium salt continuously precipitated out on the sides of the stalk as the solutions evaporate, however the calcium and magnesium solutions show almost no precipitation on the exterior portion of the stalk. To understand why, we autopsied the stalks after the evaporation experiments and took SEM images of the center of a cross section of the stalk cut at a location close to the surface of the bulk water. As shown in Figure 3B, calcium and magnesium salts formed thick salt films within the stalk, leaving very little open space. On the other hand, the sodium and potassium salts tended to form clusters around the cotton fibers, leaving the pores open and available for water transport. Cross sections imaged at other sections of the stalk are shown in Supplementary Figure S1A−D, and also confirm these findings. The morphology of salt found in the stalks is consistent throughout, but the amount of deposited salt decreases from bottom to the top of the stalk, confirming that accumulation of salt at the bottom prevents the salts from reaching the top by blocking the transport pathways. These results indicate that the key reason for the low evaporative flux seen with calcium and magnesium salts is accumulation of salt within the pores that subsequently blocks the transport of solutions.

The horizontal distribution of salts across the cross-section of the stalk is further analyzed by optical (Figure 3C) as well as SEM (Figure 3D) imaging. As illustrated in Figure 3C, the macroscopic distribution of calcium salt was quite uniform across the entire surface, meanwhile the sodium salt only severely deposited near the edges of the stalk, leaving the center region relatively open. Note that magnesium and potassium salts behave similarly to calcium and sodium salts, respectively. However, although the macroscopic distribution of magnesium and calcium salts are similar, a closer examination of the salt structure near the edge of the stalk using SEM shows some differences. As shown in Figure 3D, the calcium salt leaves larger openings than the magnesium salt in the edge region, indicating that magnesium salts can cause more severe pore blockage than calcium salts. This helps explain why the magnesium solution exhibited a much lower evaporative flux (0.35 kg m^{-2} h^{-1}) than calcium. Another difference between the two can be seen in Supplementary Movie S1, which reflects the highly deliquescent nature of magnesium chloride. Some salt precipitates out of the magnesium stalk on the first day, but then is quickly reabsorbed back into the stalk as it absorbs moisture from the air and as more water is entrained within the stalk. This behavior is not seen in the stalk in the calcium solution and

https://doi.org/10.1021/acs.est.4c08151
Environ. Sci. Technol. 2025, 59, 892−901

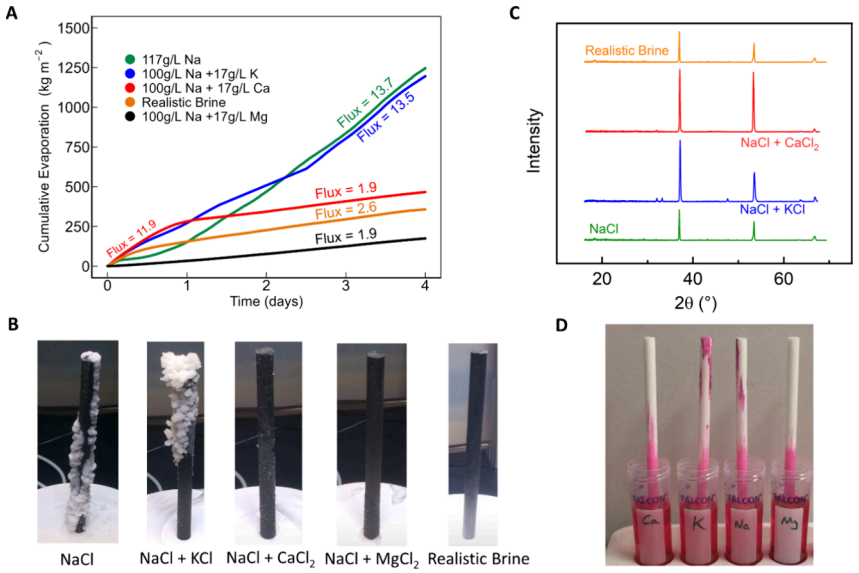

Figure 4. Evaporation performance of the 3D stalk in mixed solutions showing (A) evaporation rate of stalk (in kg m^{-2} h^{-1}) in mixtures containing a high NaCl concentration and lower concentrations of KCl, $MgCl_2$, or $CaCl_2$; (B) images of varying scale formation on the stalks after approximately 72 h; (C) XRD spectra of the scale scraped off the outside of each stalk; and (D) the transport of brine solutions dyed with rhodamine WT (pink) through a 3D-uncoated stalk.

reflects how the magnesium salt is absorbing additional moisture thereby dropping the evaporation rate even lower.

Effects of Mixed Brine Solutions on Evaporation Rates. To assess whether the declines in evaporation caused by divalent cations extend to more realistic brine conditions, we performed a series of experiments with mixed solutions containing high sodium (major ion) concentrations plus a low concentration of the other cations as minor ions. The counterion is chloride for all the conditions. To prepare each solution, we started with 100 g/L of sodium and then added an additional 17 g/L of minor ions, including Na^+ (control), K^+, Mg^{2+}, and Ca^{2+}. The 17 g/L was chosen as the concentration of the minor ions because it reflects the upper bound concentration of divalent cations typically found in natural brines.

The evaporation performances of mixed ions shown in Figure 4A are in general consistent with the results from single-salt experiments. As expected, the addition of potassium has no obvious effect on the evaporative flux, but the addition of even a small amount of calcium or magnesium results in significantly lower evaporative flux. Also, similarly to the previous experiments, the stalk in a calcium solution shows an initially high evaporation rate of 11.9 kg m^{-2} s^{-1} that gradually slows down, while that for magnesium exhibits a low flux from the very beginning. Interestingly though, the decreasing flux for calcium stabilizes at around 1.9 kg m^{-2} s^{-1}, which is the same flux as that for magnesium. The realistic brine solution contains both calcium and magnesium, and its overall trajectory is in between the solutions with 17g/L of magnesium and calcium. As seen in Figure 2E, its initial evaporation rate is 7.75 kg m^{-2} h^{-1} which is lower than the calcium stalk showing how the magnesium scales more rapidly inside the stalk. However, since the realistic brine solution has a lower concentration of magnesium (9.6 g/L), the evaporation rate does not drop to its lowest extent until the calcium, which has slower dynamics, also scales inside the stalk. Interestingly, this process is faster than in the stalk with only calcium, likely due to the fact that the calcium only has to fill in the remaining pores in between the magnesium layer. These results indicate that it is indeed the presence of calcium and magnesium ions in the brine that causes the large drop in flux that was previously discussed.

Similarly to what we observed in single-salt experiments, the presence of divalent cations inhibited the formation of scales on the surface of the stalk. Both the images in Figure 4B and video in Supplementary Movie S2 show that even though the NaCl concentration is the same for all of the solutions, the amount of NaCl scale formed on the stalk surface was significantly less in the presence of calcium or magnesium. This suggests that the divalent cations, even at a much lower concentration, can still inhibit water transport by precipitating out within the stalk. To confirm this hypothesis, we used XRD to characterize the composition of salts scraped from the surface of each stalk. Note that we did not manage to scrape enough salt from the experiments with the mixture of NaCl + $MgCl_2$ for XRD analysis. As shown in Figure 4C, the scale formed on the stalk for the realistic brine and NaCl + $CaCl_2$ mixture are the same as that of the pure NaCl, showing no signals from $CaCl_2$ or $MgCl_2$. This proves that divalent cations do not have a chance to precipitate out of the stalk at all.

To further confirm the water transport mechanism, a qualitative experiment was done using an uncoated stalk with solutions containing pink rhodamine-WT dye. As shown in Figure 4D and Supplementary Movie S3, during the evaporation process, the sodium and potassium solutions quickly move up the stalk while the magnesium and calcium solutions never reach over halfway, even after 14 days. Although this does not perfectly represent the stalk used in the experiments, it still serves as a useful method for illustrating the evaporation mechanisms. This experiment was replicated with undyed water, using thermal images to determine the water levels. The outcome, shown in Figure S2 is the same, verifying that this phenomenon is not caused by any interaction between functional groups in our material or in the dye with the divalent cations. These results confirm how

https://doi.org/10.1021/acs.est.4c08151
Environ. Sci. Technol. 2025, 59, 892−901

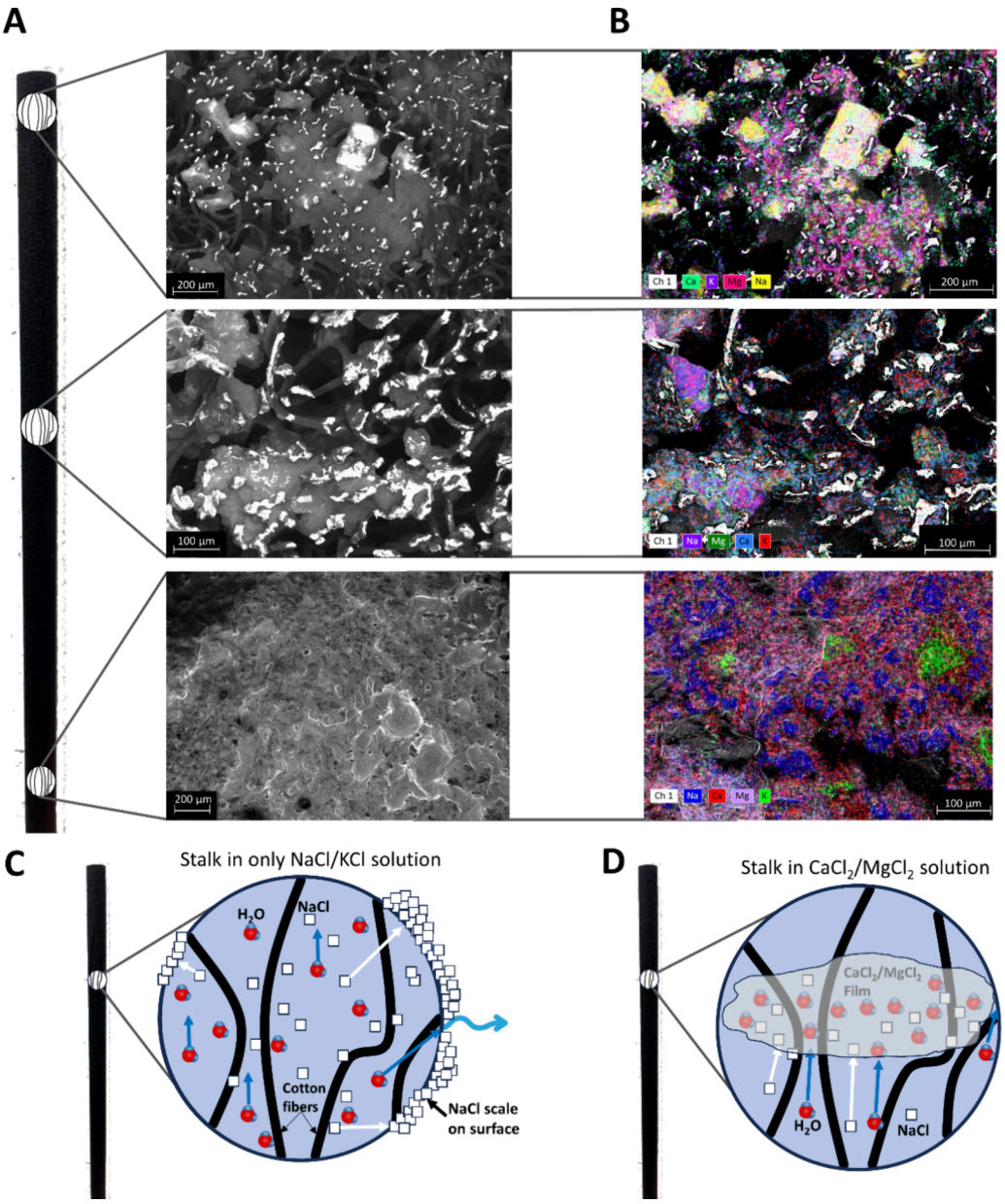

Figure 5. Water transport implications of scaling showing (A) SEM images of stalk from the realistic brine experiment as a function of height and (B) SEM/EDS image of the cross sections of the stalk, and conceptual diagrams of the scaling mechanism showing (C) a vertical cross-section of the stalk in a solution with only monovalent cations and (D) a vertical cross-section of the stalk in a solution with divalent cations.

the divalent salts block the water transport pathways as they form films across the stalk.

Summarizing the Effects of Divalent Cations in the Evaporation of Realistic Brines. To summarize the effects of divalent cations in solar evaporation of brine, we used SEM and EDS to closely examine the internal structure of a 3D stalk after evaporating the realistic brine solution. The results in Figure 5A,B show that near the water interface of the stalk, there is a large agglomeration of salt that forms. This film is made up of a mixture of magnesium and calcium with sodium and potassium entrained in the salt structure. This illustrates why in the previous samples with mixtures of cations, sodium and potassium do not form scale on the exterior of the stalk. Instead, they are caught in the film of magnesium or calcium and remain inside of the stalk. This works to block the water pathways through the stalk and reflects how even small amounts of the divalent cations can cause large effects to evaporation by entraining the other salts in the solution and blocking the pores in the stalk.

Figure 5C,D shows conceptual diagrams of the process. For sodium and potassium ions, as they move through the stalk, the water evaporates at the surfaces and then the cations start to precipitate and move out to the stalk surface, thereby leaving the water transport pathways inside the stalk open. However, for the divalent cations, as the water evaporates, they form large films across the stalk. Since calcium and magnesium chloride are both highly hygroscopic, with much higher dehydration energies than sodium or potassium these films effectively entrain water and monovalent cations within the structure and leave no pathways for water transport open. The divalent salts, therefore, prevent the evaporation of the water

https://doi.org/10.1021/acs.est.4c08151
Environ. Sci. Technol. 2025, 59, 892−901

that they entrain and prevent additional water and salts from migrating up the stalk to evaporate.

Future Outlook. This study evaluated the effect of brine solutions with mixtures of monovalent and divalent cations on the evaporation performance of a 3D solar evaporation material. We found that a 3D GO stalk with high porosity, hydrophilicity, and solar absorbance can be produced using a simple, scalable method. This material works to enhance the evaporation efficiency of water and sodium chloride solutions by over 100 times versus the solution evaporating alone. However, we found that when solutions containing any concentration of divalent cations (even with only chloride anions) are evaporated, the evaporative flux drops without the formation of any visible scale on the surface. The chloride salts of divalent cations are highly soluble and have not typically been considered scale forming chemicals in membrane separation or other water treatment systems. These observed severe drops in flux would cause issues for most solar evaporator materials deployed in the field when exposed to realistic brine mixtures since there are few brines that do not contain small amounts of calcium or magnesium chloride. To study the cause of this phenomenon, we investigated the interior of the stalk and found that calcium and magnesium form films across the inside of the stalk that work to block water transport thereby significantly lowering the evaporation rate of the solution.

The results of this work have numerous important implications for interfacial solar evaporation research. First, it underscores the importance of testing nonsodium ions when assessing the suitability of a material for solar evaporation. In most brines found throughout the world, there are significant concentrations of interfering cations which—as demonstrated—can cause significant impacts to the solar evaporation process. Therefore, in order to fully assess the feasibility of a material, the impact of divalent cations must be considered. This work also emphasizes the importance of long-term evaporation studies when testing a material. Many of the most profound effects were observed after 24 h or even longer. As resource recovery applications from brines with high concentrations of calcium and magnesium become more prominent, there is a need for the development of mitigation methods specifically targeted at reducing the effects of divalent cations on evaporation.

These mitigation methods can include extensions of previous methods that have addressed sodium chloride scaling. For example, salt-free systems can be designed which use membranes or other interventions to prevent divalent cations from reaching the evaporator surface. They can also include methods such as pretreatment of brines to induce the precipitation of the divalent cations, thereby lowering the concentration that reaches the solar evaporator. For solar evaporation systems with no intermediates between the brines and the evaporators, attention should be focused on the internal structures. Materials with different pore geometries should be investigated and assessed in terms of their ability to allow for continued water transport in the presence of divalent cations. This can be done with the aid of methods such as 3D printing which allow for more efficient testing of different materials and geometries. In all, new research attention is needed to develop and assess comprehensive mitigation methods for divalent cation scaling in order to allow for solar evaporation to be used as an efficient tool for resource recovery from brines.

■ ASSOCIATED CONTENT

Supporting Information

The Supporting Information is available free of charge at https://pubs.acs.org/doi/10.1021/acs.est.4c08151.

Ionic compositions of lithium containing brines, additional cross-sectional images of the stalks, and thermal images of the uncoated stalk in different solutions (PDF)

(Supplementary Movie S1) Timelapse video of the stalks in 10% Na^+, K^+, Ca^{2+}, and Mg^{2+} solutions (MP4)

(Supplementary Movie S2) Timelapse video of stalks run in solutions with mixtures of cations (MP4)

(Supplementary Movie S3) Timelapse video of different dyed solutions evaporating through the stalks (MP4)

■ AUTHOR INFORMATION

Corresponding Author

Baoxia Mi − *Department of Civil and Environmental Engineering, University of California, Berkeley, Berkeley, California 94720, United States;* orcid.org/0000-0003-3185-1820; Phone: +1-510-664-7446; Email: mib@berkeley.edu

Authors

Aydin F. Eskafi − *Department of Civil and Environmental Engineering, University of California, Berkeley, Berkeley, California 94720, United States*

Casey De Finnda − *Department of Civil & Environmental Engineering, UC Davis, Davis, California 95616, United States;* orcid.org/0000-0002-0520-5430

Christopher A. Garcia − *Department of Chemical and Biomolecular Engineering, University of California, Berkeley, Berkeley, California 94720, United States*

Complete contact information is available at: https://pubs.acs.org/10.1021/acs.est.4c08151

Notes

The authors declare no competing financial interest.

■ ACKNOWLEDGMENTS

This material is based upon work supported by the National Science Foundation Graduate Research Fellowship Program under grant no. DGE-2146752. Any opinions, findings, and conclusions or recommendations expressed in this material are those of the authors and do not necessarily reflect the views of the National Science Foundation. Work at the Molecular Foundry was supported by the Office of Science, Office of Basic Energy Sciences, of the U.S. Department of Energy under contract no. DE-AC02-05CH11231. We also thank Kelly Conway at the University of California, Berkeley for assistance with SEM images.

■ REFERENCES

(1) Finnerty, C. T. K.; Menon, A. K.; Conway, K. M.; Lee, D.; Nelson, M.; Urban, J. J.; Sedlak, D.; Mi, B. Interfacial Solar Evaporation by a 3D Graphene Oxide Stalk for Highly Concentrated Brine Treatment. *Environ. Sci. Technol.* **2021**, *55* (22), 15435−15445.

(2) Bu, Y.; Zhou, Y.; Lei, W.; Ren, L.; Xiao, J.; Yang, H.; Xu, W.; Li, J. A Bioinspired 3D Solar Evaporator with Balanced Water Supply and Evaporation for Highly Efficient Photothermal Steam Generation. *Journal of Materials Chemistry A* **2022**, *10* (6), 2856−2866.

(3) Yu, S.; Gu, Y.; Chao, X.; Huang, G.; Shou, D. Recent Advances in Interfacial Solar Vapor Generation: Clean Water Production and Beyond. *Journal of Materials Chemistry A* **2023**, *11* (12), 5978−6015.
(4) Finnerty, C.; Zhang, L.; Sedlak, D. L.; Nelson, K. L.; Mi, B. Synthetic Graphene Oxide Leaf for Solar Desalination with Zero Liquid Discharge. *Environ. Sci. Technol.* **2017**, *51* (20), 11701−11709.
(5) Wu, P.; Wu, X.; Wang, Y.; Xu, H.; Owens, G. A Biomimetic Interfacial Solar Evaporator for Heavy Metal Soil Remediation. *Chemical Engineering Journal* **2022**, *435*, No. 134793.
(6) Wu, L.; Dong, Z.; Cai, Z.; Ganapathy, T.; Fang, N. X.; Li, C.; Yu, C.; Zhang, Y.; Song, Y. Highly Efficient Three-Dimensional Solar Evaporator for High Salinity Desalination by Localized Crystallization. *Nat. Commun.* **2020**, *11* (1), 521.
(7) Fan, X.; Peng, Y.; Lv, B.; Yang, Y.; You, Z.; Song, C.; Xu, Y. A Siphon-Based Spatial Evaporation Device for Efficient Salt-Free Interfacial Steam Generation. *Desalination* **2023**, *552*, No. 116442.
(8) Wang, Y.; Shang, Y.; Sun, X.; Yang, Q.; Zhang, Y. Enhancing Freshwater Production via Customizable and Highly Efficient Solar-Driven Seawater Desalination. *ACS Appl. Mater. Interfaces* **2023**, *15* (34), 40595−40605.
(9) Chen, S.; Sun, L.; Huang, Y.; Yang, D.; Zhou, M.; Zheng, D. Biochar-Based Interfacial Evaporation Materials Derived from Lignosulfonate for Efficient Desalination. *Carbon Neutralization* **2023**, *2* (4), 494−509.
(10) Zhang, Y.; Watanabe, H.; Shi, J.; Morikawa, H.; Zhu, C. Innovative Mushroom-like Hemp-Based Evaporators Enhanced by Biochar for Efficient Seawater Desalination. *Desalination* **2024**, *576*, No. 117342.
(11) Qiao, H.; Zhao, B.; Suo, X.; Xie, X.; Dang, L.; Yang, J.; Zhang, B. The Biochar Derived from Carp for High-Efficiency Solar Steam Generation and Water Purification. *Global Challenges* **2022**, *6* (1), No. 2100083.
(12) Yang, L.; Li, N.; Guo, C.; He, J.; Wang, S.; Qiao, L.; Li, F.; Yu, L.; Wang, M.; Xu, X. Marine Biomass-Derived Composite Aerogels for Efficient and Durable Solar-Driven Interfacial Evaporation and Desalination. *Chemical Engineering Journal* **2021**, *417*, No. 128051.
(13) Li, H.; Zhu, W.; Li, M.; Li, Y.; Kwok, R. T. K.; Lam, J. W. Y.; Wang, L.; Wang, D.; Tang, B. Z. Side Area-Assisted 3D Evaporator with Antibiofouling Function for Ultra-Efficient Solar Steam Generation. *Adv. Mater.* **2021**, *33* (36), No. 2102258.
(14) Cao, N.; Lu, S.; Yao, R.; Liu, C.; Xiong, Q.; Qin, W.; Wu, X. A Self-Regenerating Air-Laid Paper Wrapped ASA 3D Cone-Shaped Janus Evaporator for Efficient and Stable Solar Desalination. *Chemical Engineering Journal* **2020**, *397*, No. 125522.
(15) Shi, Y.; Zhang, C.; Li, R.; Zhuo, S.; Jin, Y.; Shi, L.; Hong, S.; Chang, J.; Ong, C.; Wang, P. Solar Evaporator with Controlled Salt Precipitation for Zero Liquid Discharge Desalination. *Environ. Sci. Technol.* **2018**, *52* (20), 11822−11830.
(16) Xu, N.; Li, J.; Finnerty, C.; Song, Y.; Zhou, L.; Zhu, B.; Wang, P.; Mi, B.; Zhu, J. Going beyond Efficiency for Solar Evaporation. *Nat. Water* **2023**, *1* (6), 494−501.
(17) Menon, A. K.; Haechler, I.; Kaur, S.; Lubner, S.; Prasher, R. S. Enhanced Solar Evaporation Using a Photo-Thermal Umbrella for Wastewater Management. *Nat. Sustain* **2020**, *3* (2), 144−151.
(18) Swain, B. Recovery and Recycling of Lithium: A Review. *Sep. Purif. Technol.* **2017**, *172*, 388−403.
(19) International Energy Agency *Role of Critical Minerals in Clean Energy Transitions*; IEA. https://www.iea.org/reports/the-role-of-critical-minerals-in-clean-energy-transitions
(20) Zhang, S.; Wei, X.; Cao, X.; Peng, M.; Wang, M.; Jiang, L.; Jin, J. Solar-Driven Membrane Separation for Direct Lithium Extraction from Artificial Salt-Lake Brine. *Nat. Commun.* **2024**, *15* (1), 238.
(21) Chen, X.; Yang, M.; Zheng, S.; Temprano-Coleto, F.; Dong, Q.; Cheng, G.; Yao, N.; Stone, H. A.; Hu, L.; Ren, Z. J. Spatially Separated Crystallization for Selective Lithium Extraction from Saline Water. *Nat. Water* **2023**, *1* (9), 808−817.
(22) Sosso, G. C.; Chen, J.; Cox, S. J.; Fitzner, M.; Pedevilla, P.; Zen, A.; Michaelides, A. Crystal Nucleation in Liquids: Open Questions and Future Challenges in Molecular Dynamics Simulations. *Chem. Rev.* **2016**, *116* (12), 7078−7116.
(23) Liu, G.; Chen, T.; Xu, J.; Yao, G.; Xie, J.; Cheng, Y.; Miao, Z.; Wang, K. Salt-Rejecting Solar Interfacial Evaporation. *Cell Reports Physical Science* **2021**, *2* (1), No. 100310.
(24) Tong, T.; Wallace, A. F.; Zhao, S.; Wang, Z. Mineral Scaling in Membrane Desalination: Mechanisms, Mitigation Strategies, and Feasibility of Scaling-Resistant Membranes. *J. Membr. Sci.* **2019**, *579*, 52−69.
(25) Shahidzadeh-Bonn, N.; Rafaï, S.; Bonn, D.; Wegdam, G. Salt Crystallization during Evaporation: Impact of Interfacial Properties. *Langmuir* **2008**, *24* (16), 8599−8605.
(26) Mucha, M.; Jungwirth, P. Salt Crystallization from an Evaporating Aqueous Solution by Molecular Dynamics Simulations. *J. Phys. Chem. B* **2003**, *107* (33), 8271−8274.
(27) Misyura, S. Y. Evaporation and Heat Transfer of Aqueous Salt Solutions during Crystallization. *Applied Thermal Engineering* **2018**, *139*, 203−212.
(28) McBride, S. A.; Girard, H.-L.; Varanasi, K. K. Crystal Critters: Self-Ejection of Crystals from Heated, Superhydrophobic Surfaces. *Science Advances* **2021**, *7* (18), No. eabe6960.
(29) Zang, L.; Finnerty, C.; Zheng, S.; Conway, K.; Sun, L.; Ma, J.; Mi, B. Interfacial Solar Vapor Generation for Desalination and Brine Treatment: Evaluating Current Strategies of Solving Scaling. *Water Res.* **2021**, *198*, No. 117135.
(30) Li, C.; Cao, Y.; Tian, X.; Shen, Y.; Xiao, J.; Huang, W.; Wang, H.; Liu, Z. Dual-Hydrophilic Janus Evaporator for Long-Term and Efficient Bimode Solar Evaporation. *Chemical Engineering Journal* **2023**, *461*, No. 141954.
(31) Liu, Z.; Qing, R.-K.; Xie, A.-Q.; Liu, H.; Zhu, L.; Chen, S. Self-Contained Janus Aerogel with Antifouling and Salt-Rejecting Properties for Stable Solar Evaporation. *ACS Appl. Mater. Interfaces* **2021**, *13* (16), 18829−18837.
(32) Zhang, L.; Wang, X.; Xu, X.; Yang, J.; Xiao, J.; Bai, B.; Wang, Q. A Janus Solar Evaporator with Photocatalysis and Salt Resistance for Water Purification. *Sep. Purif. Technol.* **2022**, *298*, No. 121643.
(33) Li, L.; He, N.; Jiang, B.; Yu, K.; Zhang, Q.; Zhang, H.; Tang, D.; Song, Y. Highly Salt-Resistant 3D Hydrogel Evaporator for Continuous Solar Desalination via Localized Crystallization. *Adv. Funct. Mater.* **2021**, *31* (43), No. 2104380.
(34) Shen, C.; Zhu, Y.; Xiao, X.; Xu, X.; Chen, X.; Xu, G. Economical Salt-Resistant Superhydrophobic Photothermal Membrane for Highly Efficient and Stable Solar Desalination. *ACS Appl. Mater. Interfaces* **2020**, *12* (31), 35142−35151.
(35) Xia, Y.; Li, Y.; Yuan, S.; Kang, Y.; Jian, M.; Hou, Q.; Gao, L.; Wang, H.; Zhang, X. A Self-Rotating Solar Evaporator for Continuous and Efficient Desalination of Hypersaline Brine. *J. Mater. Chem. A* **2020**, *8* (32), 16212−16217.
(36) Wu, X.; Wang, Y.; Wu, P.; Zhao, J.; Lu, Y.; Yang, X.; Xu, H. Dual-Zone Photothermal Evaporator for Antisalt Accumulation and Highly Efficient Solar Steam Generation. *Adv. Funct. Mater.* **2021**, *31* (34), No. 2102618.
(37) Xu, Y.; Peng, Y.; Lv, B.; Song, C.; You, Z.; Liu, Y.; Fan, X. Mineral Scaling Behavior in Typical Salt-Resistant Solar Interfacial Desalination: Edge-Preferential Crystallization *vs.* Enhanced Convection. *Chemical Engineering Journal* **2023**, *477*, No. 146899.
(38) Naghdi, B.; Heshmati, F. Z.; Mahjoub, F.; Arabpour Roghabadi, F.; Ahmadi, V.; Luo, Y.; Wang, Z.; Sadrameli, S. M. Salt Precipitation Challenge in Floating Interfacial Solar Water Desalination Systems. *Desalination* **2023**, *565*, No. 116868.
(39) An, J. W.; Kang, D. J.; Tran, K. T.; Kim, M. J.; Lim, T.; Tran, T. Recovery of Lithium from Uyuni Salar Brine. *Hydrometallurgy* **2012**, *117−118*, 64−70.
(40) Ventura, S.; Bhamidi, S.; Hornbostel, M.; Nagar, A. *Selective Recovery of Lithium from Geothermal Brines: Final Project Report*; California Energy Comission, 2020.
(41) Tran, T.; Luong, V. T. Lithium Production Processes. In *Lithium Process Chemistry*; Elsevier, 2015; pp 81−124. .

(42) Tran, K. T.; Van Luong, T.; An, J.-W.; Kang, D.-J.; Kim, M.-J.; Tran, T. Recovery of Magnesium from Uyuni Salar Brine as High Purity Magnesium Oxalate. *Hydrometallurgy* **2013**, *138*, 93−99.
(43) Rolf, J.; Cao, T.; Huang, X.; Boo, C.; Li, Q.; Elimelech, M. Inorganic Scaling in Membrane Desalination: Models, Mechanisms, and Characterization Methods. *Environ. Sci. Technol.* **2022**, *56* (12), 7484−7511.
(44) Zhang, C.; Shi, Y.; Shi, L.; Li, H.; Li, R.; Hong, S.; Zhuo, S.; Zhang, T.; Wang, P. Designing a next Generation Solar Crystallizer for Real Seawater Brine Treatment with Zero Liquid Discharge. *Nat. Commun.* **2021**, *12* (1), 998.
(45) Boryta, D.; Kullberg, T.; Thurston, A. Production of Lithium Compounds Directly from Lithium Containing Brines. US20030228251A1, 2003. https://patents.google.com/patent/US20030228251A1/en
(46) Wu, X.; Lu, Y.; Ren, X.; Wu, P.; Chu, D.; Yang, X.; Xu, H. Interfacial Solar Evaporation: From Fundamental Research to Applications. *Adv. Mater.* **2024**, *36* (23), No. 2313090.
(47) Sun, Y.; Tan, X.; Xiang, B.; Gong, J.; Li, J. Solar-Driven Interfacial Evaporation for Sustainable Desalination: Evaluation of Current Salt-Resistant Strategies. *Chemical Engineering Journal* **2023**, *474*, No. 145945.

https://doi.org/10.1021/acs.est.4c08151
Environ. Sci. Technol. 2025, 59, 892−901